# Photexcitation of Aqueous Ruthenium(II)-tris-(2,2′-bipyridine) with High-Intensity Femtosecond Laser Pulses

**A. N. Tarnovsky,[†,§] W. Gawelda,[†,‡] M. Johnson,[†,∥] C. Bressler,[†] and M. Chergui*[,†]**

*Ecole Polytechnique Fédérale de Lausanne, Laboratory of Ultrafast Spectroscopy, ISIC, BSP, CH-1015 Lausanne-Dorigny, Switzerland, and Swiss Light Source, Paul Scherrer Institut, CH-5232 Villigen, Switzerland*

*Received: July 24, 2006; In Final Form: October 3, 2006*

We report a femtosecond pump−probe study on the photochemistry of concentrated aqueous solutions of $[Ru^{II}(bpy)_3]^{2+}$, as a function of pump power (up to 2 TW/cm$^2$) at 400 nm excitation. The transient absorption spectra in the 345−660 nm range up to 1 ns time delay enable the observation of the following photoproducts: the triplet $^3$MLCT (metal-to-ligand-charge-transfer) excited state, the reduced form $[Ru^{II}(bpy)_3]^{+}$, the oxidized species $[Ru^{III}(bpy)_3]^{3+}$, and the solvated electron $e_{aq}$. The $^3$MLCT state is formed within the excitation pulse and undergoes vibrational relaxation in 3−5 ps, as evidenced by the shift of the ligand-centered (LC) absorption band below 400 nm. Even at the highest pump powers, the majority of $e_{aq}$ originates from multiphoton ionization of $[Ru^{II}(bpy)_3]^{2+}$ and not from the solvent, generating $[Ru^{III}(bpy)_3]^{3+}$ as a byproduct. At 10 ps time delay, the total concentration of the three product species is balanced by the depleted concentration of $[Ru^{II}(bpy)_3]^{2+}$, even at the highest fluences used, indicating that no further reaction products significantly contribute to the overall photochemistry. On the 100 ps time scale, most probably diffusion-controlled reduction of ground-state $[Ru^{II}(bpy)_3]^{2+}$ by solvated electrons occurs, next to recombination between $e_{aq}$ and $[Ru^{III}(bpy)_3]^{3+}$.

## I. Introduction

The photochemistry of coordination compounds and, in particular, of metal complexes that exhibit metal-to-ligand charge transfer (MLCT) transitions has been a central theme of inorganic chemistry for several decades. Ruthenium(II)-tris-(2,2′-bipyridine), $[Ru^{II}(bpy)_3]^{2+}$, has served as a prototype of d$^6$ polypyridine complexes of second-row transition metals.[1,2] Considerable efforts have been made to describe the photophysics and photochemistry of this complex.[1−12] Light absorption within the visible metal-to-ligand charge-transfer band of $[Ru^{II}(bpy)_3]^{2+}$ populates the $^1$MLCT singlet excited state, which undergoes ultrafast intersystem crossing with a near unit probability[13] to the long-lived (∼600 ns lifetime in water at ambient temperature) triplet $^3$MLCT excited state (Figure 1a, inset). In the latter state, the transferred electron is localized on one of the bpy ligands, giving rise to a $[Ru^{III}(bpy^-)(bpy)_2]^{2+}$ species in the following reaction sequence:

$$[Ru^{II}(bpy)_3]^{2+} \xrightarrow{h\nu} {}^1\text{MLCT} \quad (1)$$

$$^1\text{MLCT} \rightarrow {}^3\text{MLCT} \quad (2)$$

The dominant intramolecular decay of the $^3$MLCT state is radiationless, involving thermally activated relaxation to optically silent metal-centered excited states (so-called triplet metal-centered $^3$MC or $^3$dd states), and to high vibrational levels of the ground state.[14] Bimolecular quenching is also important for the $^3$MLCT state because of its long lifetime. The reduction and oxidation potentials of the $^3$MLCT state are large and nearly equal in magnitude (ca. 0.85 V),[1] so both oxidative and reductive quenching can occur, resulting in the formation of the reduced product $[Ru^{II}(bpy)_2(bpy^{\cdot-})]^{+}$ (later abbreviated as $[Ru^{II}(bpy)_3]^{+}$) and the oxidized product $[Ru^{III}(bpy)_3]^{3+}$.

With femtosecond photolysis pulses, peak intensities of $\sim 10^{28}-10^{30}$ photons cm$^{-2}$ s$^{-1}$ (∼0.005−0.5 TW cm$^{-2}$) are easily achievable, which lie in the range of saturation intensities for metal complexes. This may also lead to multiphoton absorption to highly excited states, which in return exhibit new deactivation pathways, for example, charge ejection. Furthermore, in concentrated samples and in molecular assemblies, cooperative effects[8,15,16] may arise, due to the high-density excitation, which are still not fully understood.

Despite the impressive literature on Ru−polypyridyl complexes, few studies have dealt with the issues of high excitation intensities and large concentrations in these systems, and these were mainly done with nanosecond pulses. Milosavijvich and Thomas[5] carried out the only such study for the case of $[Ru^{II}(bpy)_3]^{2+}$ (≤100 mM) adsorbed onto cellulose as well as in water solution. They observed that the $^3$MLCT emission obeyed a pseudo first-order decay when changing concentration of the ground-state complexes in the range 10−100 mM, and ascribed this to "catalyzed deactivation" of the excited complex by a neighboring ground-state complex. At large excitation energies (and, in consequence, large $^3$MLCT concentrations), the $^3$MLCT decay followed mixed first- and second-order kinetics attributed to the presence of both ground-state quenching and triplet−triplet annihilation. It was concluded that triplet−triplet annihilation gives rise to singly charged complexes (observed by their absorption at 520 nm) via intermolecular electron transfer.[5,16,17] Recently, however, an energy-transfer annihilation mechanism was invoked for polypyridyne Ru(II) complexes

* Corresponding author. E-mail: majed.chergui@epfl.ch.
† Ecole Polytechnique Fédérale de Lausanne.
‡ Paul Scherrer Institute.
§ Present address: Department of Chemistry, Center for Photochemical Sciences, Bowling Green State University, Bowling Green, OH 43403.
∥ Present address: Allgemeine Energie, Paul Scherrer Institute, CH-5232 Villigen, Switzerland.

10.1021/jp064696f CCC: $33.50 
Published on Web 12/08/2006

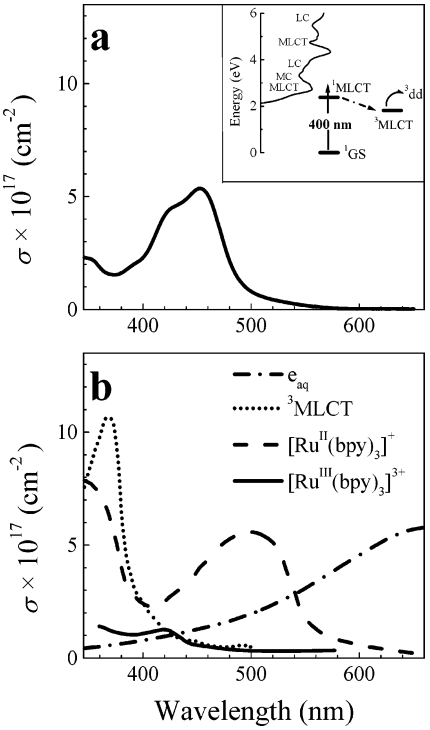


**Figure 1.** (a) Absorption spectrum of aqueous $[Ru^{II}(bpy)_3]^{2+}$. The inset shows a simplified energy level diagram of the lowest excited states together with the absorption spectrum from the singlet ground state $^1$GS. The assignment of the MC, LC, and MLCT bands (see text) is adopted from ref 1. (b) Absorption spectra of the product species involved in the photolysis of $[Ru^{II}(bpy)_3]^{2+}$ in water solutions: $^3$MLCT state,[37] $[Ru^{II}(bpy)_3]^+$,[44] $[Ru^{III}(bpy)_3]^{3+}$,[3] and $e_{aq}$.[43] The spectra are shown in the spectral range investigated in this work.

bound to polystyrene.[8] Nanosecond laser intensity effects have been investigated in dilute aqueous solutions by Thompson et al.[18] and by Goez et al.[19,20] In the latter case, no product other than $^3$MLCT was observed, even at the highest intensities of the 532 nm excitation pulse. Upon excitation at 308 and 355 nm, the solvated electron was observed and its occurrence explained by sequential two-photon photoionization of $[Ru^{II}(bpy)_3]^{2+}$ via the $^3$MLCT intermediate.[19,20] It was also suggested that the same nanosecond photolysis pulse drives the excited-state reduction of a ($[Ru^{III}(bpy)_3]^{3+}$) byproduct by the solvent $H_2O$, thereby regenerating the $^3$MLCT species. However, this interpretation is very different from that of Thompson et al.,[18] who, following high-power 355 nm photolysis of $[Ru^{II}(bpy)_3]^{2+}$, proposed a photochemical route with formation of a long-lived complex (lifetime ca. 80 $\mu$s) with a monodentate ligand.

This brief review shows that the behavior of $[Ru^{II}(bpy)_3]^{2+}$ in concentrated solutions under high-intensity femtosecond excitation is by no means clear and, given the many potential applications of Ru−polypyridine complexes, it deserves further investigation, which is the purpose of this contribution. Here, we determine product concentrations of the light-triggered and subsequent dark reactions up to 1 ns time delay, and disentangle, in a systematic way, the ensuing processes. Previously, femtosecond laser studies[6,9,12,21] within the first picosecond revealed rich dynamics in the initially populated $^1$MLCT and $^3$MLCT states, and microsecond-to-millisecond studies[1,5,18,22,23] unraveled the diffusion-controlled and slower reactions involving photolysis products of this complex, but much less is known about the intermediate time scale investigated in the present paper. Our results can be embedded into a rather simple picture of known reaction products without invoking unknown dark channels or exotic reaction intermediates.[18] They also demonstrate the "robustness" of $[Ru^{II}(bpy)_3]^{2+}$ under high-intensity laser excitation.

## II. Experimental Section

**Materials.** Tris(2,2′-bipyridine)-ruthenium(II) chloride hexahydrate was used as received from Fluka. Deionized water was used as the solvent. Solutions of $[Ru^{II}(bpy)_3]^{2+}$ (0.4, 10, and 20 mM) at 20 °C were flown through a 100 $\mu$m thick jet to ensure the complete renewal of the sample between consecutive laser pulses. No attempt was made to deoxygenate the solutions under investigation, because quenching by aqueous $O_2$ at 20 °C ($[O_2] = 1.39 \times 10^{-3}$ M$^{-1}$)[24] is too slow to influence the reactions on a subnanosecond time scale. Static UV−vis absorption spectra of the samples were measured using a Perkin-Elmer LAMBDA-35 spectrophotometer.

**Transient Absorption Measurements.** Our transient absorption spectrometer is based on a 1 kHz Ti:sapphire pumped regenerative amplifier system producing ~100 fs, 0.85 mJ pulses centered at ~800 nm. Briefly, a white-light continuum (wlc) probe beam was generated by focusing a small part of the fundamental output into a 2 mm thick $CaF_2$ window. Excitation at 400 nm with pulse energies up to 115 $\mu$J were obtained by frequency doubling 90% of the fundamental 800 nm output. The diameters (fwhm) of the excitation and probe beams at the sample position were measured via the knife-edge technique and varied in the range of $d = 180-220$ $\mu$m (depending on the utilized lens and its distance to the sample), and set to ~60 $\mu$m, respectively. The relative polarization of the excitation and probe electric field vectors was either orthogonal or set to the magic angle (54.7°). A charge-coupled device (and sometimes a single diode array) was used to acquire transient absorption spectra in the 350−650 nm range. The group-velocity dispersion (chirp) of the wlc was measured in a neat water jet exploiting the two-photon absorption[25,26] and the cross-phase modulation signals around time zero.[26,27] The transient absorption spectra measured at short delay times ($t < 10$ ps) were corrected for the chirp. A strong emission feature[27] (fwhm duration 195 ± 15 fs) at 470 nm in liquid water due to the Raman-active symmetric stretch mode of $H_2O$ ($\nu_1 = 3490$ cm$^{-1}$) delivered a cross-correlation signal between pump and probe pulses. An excitation pulse width of $\tau_p = 135$ fs (fwhm) is inferred assuming Gaussian-shaped pump and probe pulses of equal pulse width. The peak irradiance $I_0$ and the fluence $E_0$ of the 400-nm excitation pulses are obtained from the expressions for Gaussian-shaped pulses in both time and space:[28]

$$I_0 = E8(\pi^{-1}\ln 2)^{3/2}/(h\nu_{400}d^2\tau_p), \quad E_0 = E4(\ln 2)/(\pi d^2)$$

where $E$ is the total pulse energy, and $h\nu_{400}$ is the energy of a 400-nm photon (=3.1 eV). The largest $E_0$ in this study was 0.31 J cm$^{-2}$ ($I_0 = 4.35 \times 10^{30}$ photons cm$^{-2}$ s$^{-1}$), corresponding to a power of 2.15 TW cm$^{-2}$.

**Data Analysis Procedures.** The transient absorption spectra $\Delta A_\lambda{}^t$ acquired at delay times $t \geq 10$ ps were fitted to the absorption spectra of the reactant ($[Ru^{II}(bpy)_3]^{2+}$) and of the formed product species, with their concentrations being the only fit parameters via

$$\Delta A_\lambda{}^t = \frac{10^{-3} N_A l}{\ln 10} \sum_{i=1}^{5} \Delta c^t(i)\sigma_\lambda(i) \qquad (3)$$

Here, $N_A = 6.022 \times 10^{23}$ mol$^{-1}$ is Avogadro's constant, $l$ is the sample thickness (in cm), and $\sigma_\lambda(i)$ are the absorption cross-sections of the involved species $i$ corresponding to ($[Ru^{II}$-

$(bpy)_3]^{2+}$, $^3$MLCT, $e_{aq}$, $[Ru^{II}(bpy)_3]^+$, and $[Ru^{III}(bpy)_3]^{3+}$), as displayed in Figure 1. The fit parameters $\Delta c^t(i)$ are defined as $\Delta c^t(i) = c^t(i) - c^{t<0}(i)$, where $c^{t<0}(i)$ and $c^t(i)$ are the concentrations of the reactant and of the products at time $t$ after photoexcitation, respectively. The initial reactant concentration $c^{t<0}([Ru^{II}(bpy)_3]^{2+})$ is equal to that of the prepared solution (no products prior to photoexcitation).

For the above treatment, it is necessary to know the absolute absorption cross-section of the involved species, whose spectra are shown in Figure 1b. As the spectrum of $[Ru^{III}(bpy)_3]^{3+}$ was reported only from 360 to 600 nm, we have set $\sigma_{360} = 1.4 \times 10^{-17}$ cm$^2$ in the 346−360 nm interval and $\sigma_{600} = 0.35 \times 10^{-17}$ cm$^2$ in the 600−660 nm interval. The absolute cross-section of the $^3$MLCT state reported in the literature is somewhat contradictory. For production of only the $^3$MLCT species at the expense of the ground-state $[Ru^{II}(bpy)_3]^{2+}$ species, eq 3 reduces to:

$$\Delta A_\lambda = \frac{10^{-3} N_A l}{\ln 10} \Delta c\{\sigma_\lambda(^3\text{MLCT}) - \sigma_\lambda([Ru^{II}(bpy)_3]^{2+})\} \qquad (4)$$

where $\Delta c$ is the (identical) concentration change of both species. Once either the absolute value of $\sigma(^3$MLCT) at a single wavelength or the concentration of the excited-state species is known by means of photochemical methods,[29] the transient absorption spectrum can be converted to an absolute cross-section spectrum. The $\sigma_{368}$ values at the $^3$MLCT absorption maximum in $H_2O$ lie around $\sim (8.5-11.0) \times 10^{-17}$ cm$^{-2}$.[4,30−39] Here, we use the spectrum reported by ref 37, which agrees with several of the above cited. As this spectrum was reported only for $\lambda \leq 500$ nm, we extended it to 660 nm using eq 5 and the $\Delta A$ spectrum measured for the 0.4 mM sample at low power. We obtain a roughly constant $\sigma(^3\text{MLCT}) = 0.455 \times 10^{-17}$ cm$^2$ in this range, which reasonably agrees with the published values.[32,38] We hereby neglect a weakly pronounced spectral dependence in the 500−660 nm range, which does not alter the fit results shown below.

### III. Results and Data Analysis

**Measurements in Neat Water.** Because we are concerned with the behavior of $[Ru^{II}(bpy)_3]^{2+}$ under high-intensity excitation, it is important to first assess the contribution of photogenerated solvated electrons from the pure water solvent. Excitation of neat $H_2O$ with high-intensity 400 nm, 135 fs pulses yields a broad absorption band, centered around 700 nm, due to solvated electrons, which are formed by three-photon ionization of water molecules:[40,41]

$$H_2O \xrightarrow{n \times h\nu} H_2O^+ + e_{aq} \qquad (5)$$

The solvated electrons exhibit practically no decay within 1 ns, and their concentration shows a nonlinear dependence on the excitation fluence ($E_0$) to the power of ∼2.5 (not shown). At the largest irradiance of 2.15 TW cm$^{-2}$ ($E_0 = 0.31$ J cm$^{-2}$), we observe their strongest absorption (corresponding to $\Delta c_{max}^{100ps} = 1.35$ mM averaged over the 100 $\mu$m thick water jet). Energy fluences smaller than 0.028 J cm$^{-2}$ produce no measurable signal ($\Delta A_{660} < 8 \times 10^{-4}$). The lack of substantial recombination on the 1 ns time scale and the nearly cubic excitation energy dependence of the $e_{aq}$ concentration are consistent with earlier studies on water photoionization with ∼150 fs laser pulses at a similar wavelength.[41] However, a substantial (tens of °C) heating of water was suggested for intensities >1 TW cm$^{-2}$ based on a red shift in the electron absorption spectrum.[40,41] The range

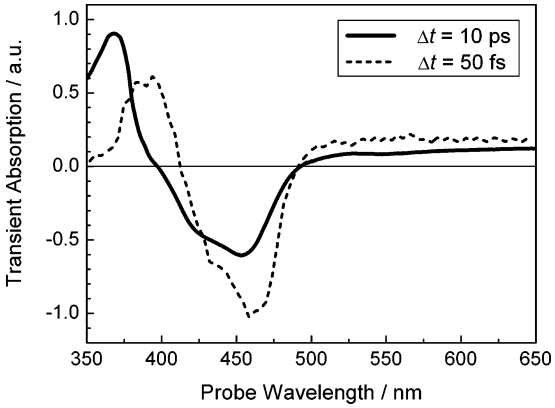


**Figure 2.** Transient absorption spectrum of aqueous $[Ru^{II}(bpy)_3]^{2+}$ 50 fs and 10 ps after photoexcitation (indicated). The decrease of the bleach and of the electron absorption above 500 nm is probably due to ultrafast geminate recombination. Note the blue shift of ∼0.25 eV of the excited-state absorption due to relaxation within the $^3$MLCT manifold. Correction for the group velocity dispersion has been performed for wavelengths >380 nm.

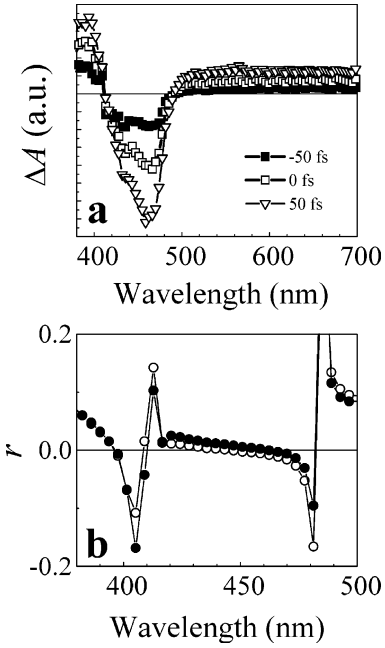


**Figure 3.** Aqueous $[Ru^{II}(bpy)_3]^{2+}$ (10 mM) excited with 400 nm photolysis pulses of 135 fs duration. (a) Ultrafast transient absorption spectra at magic angle, within the photolysis pulse and incident fluence ($E_0$) of 0.028 J cm$^{-2}$. The time delays are indicated in the plot. (b) Wavelength dependence of the anisotropy at 20 ps (○) and 100 ps (●) time delay, for $E_0 = 0.12$ J cm$^{-2}$.

345−660 nm in which the $\Delta A$ spectra were measured in our work (the irradiance range 1−1.9 TW cm$^{-2}$) is sufficient for the comparison. The relative $\Delta A$ amplitudes are clearly different from the experimental spectrum of photoelectrons observed 50 ps after the excitation of water with a 1.9 TW cm$^{-2}$ pulse,[40,41] or from the spectrum of the thermalized hydrated electrons in 80 °C water. Both the spectrum of $e_{aq}$ at room temperature and the spectrum of the photoelectrons averaged along the path of the beam (see Figure 5 of ref 41) agree with our spectra.

**Measurements on Aqueous $[Ru^{II}(bpy)_3]^{2+}$.** The photolysis wavelength 400 nm lies on the high-energy side of the broad MLCT band of $[Ru^{II}(bpy)_3]^{2+}$, which peaks at 453 nm in water (Figure 1a). Figures 2−5 show the transient absorption spectra of aqueous $[Ru^{II}(bpy)_3]^{2+}$ (10 mM) at different pump−probe time delays and for varying pump fluences ($E_0$). Figure 2

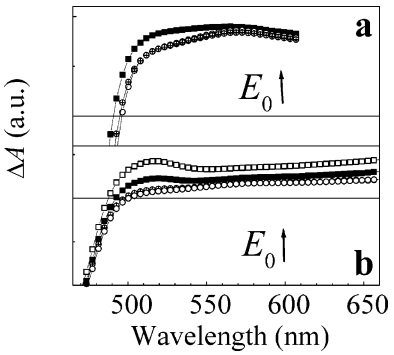


**Figure 4.** Transient absorption spectra of aqueous $[Ru^{II}(bpy)_3]^{2+}$ (10 mM) at magic angle, for different excitation energies $E_0$, recorded immediately one after the other with all other conditions being identical. (a) $\Delta A$ curves at 75 ± 30 fs time delay, normalized at the $\Delta A_{660}$ point. (b) $\Delta A$ curves at 1 ns time delay, normalized at the $\Delta A_{450}$ point. The $\Delta A$ curves from top to bottom in both panels correspond to the following excitation energies $E_0$ (in J cm$^{-2}$): 0.15 (shown only in the panel b), 0.055, 0.028, and 0.012.

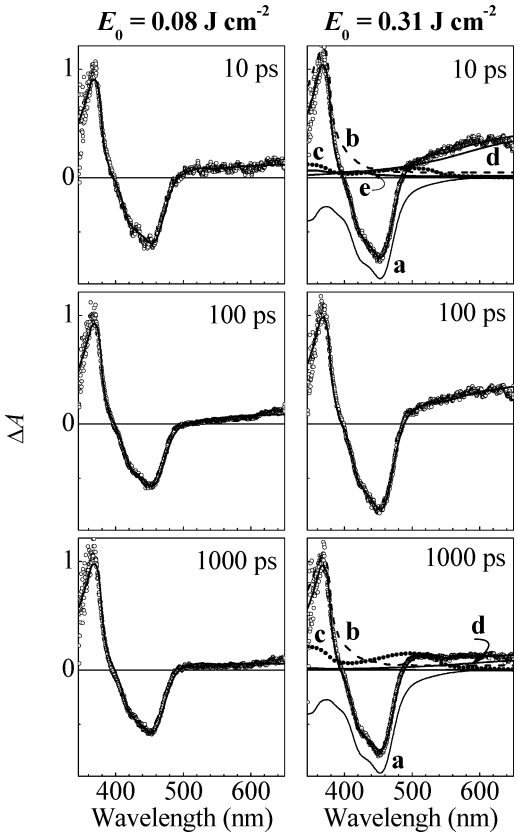


**Figure 5.** The measured transient absorption $\Delta A$ spectra (○) upon 400 nm photolysis of aqueous $[Ru^{II}(bpy)_3]^{2+}$ (10 mM) and their fits (shown as solid thin lines) to the steady-state absorption spectra of the involved species. Time delays are shown in the top left corners of each window. In the right panel, the individual steady-state product spectra obtained by spectral deconvolution of the measured $\Delta A$ spectra using eq 3 are shown: $[Ru^{II}(bpy)_3]^{2+}$ (a), $^3$MLCT (b), $[Ru^{II}(bpy)_3]^{+}$ (c), $e_{aq}$ (d), $[Ru^{III}(bpy)_3]^{3+}$ (e).

displays the depleted absorbance between 400 and 500 nm, the induced absorbance below 400 nm, due to the $^3$MLCT excited-state absorption, and in the wavelength region 500−660 nm, due to the solvated electron. These features differ to some extent between 50 fs and 10 ps: (a) the amplitudes of the bleach component and the electron absorption change, most probably due to immediate geminate recombination, which would re-form the ground-state complex; (b) the $^3$MLCT excited-state absorption below 400 nm, due to the ligand-centered (LC) band, narrows and shifts to the blue, most probably due to electronic-vibrational relaxation in the triplet manifold. The ultrafast $\Delta A$ spectra ($-50$ fs $\leq \Delta t \leq$ 50 fs) provide further insight into the initial formation of reaction products (Figures 2 and 3a). Indeed, the absorption of the nascent photoelectron (above 500 nm) is already present, along with the substantial absorption from vibrationally hot $^3$MLCT molecules. The latter can be rationalized by the extremely rapid intersystem crossing (∼15 fs), which in addition occurs at constant energy, as recently measured by femtosecond fluorescence up-conversion techniques.[12] The evolution of the absorption below 400 nm occurs with a time constant of 3.5 ps at low $E_0$, increasing to 5 ps at the highest $E_0$ used, as measured at fixed wavelengths (not shown). Our results differ from those of Wallin et al.,[10] who found no evolution of the band between 1 and 1000 ps, suggesting that the relaxation within the triplet manifold occurs in <1 ps.

Comparing the short time scale $\Delta A$ spectra measured for increasing $E_0$ and normalized to the electron absorbance, we notice an additional absorption feature in the 510−530 nm region as early as 75 fs after excitation (Figure 4a), which is also seen as a shoulder band at 510 nm at longer time delays (Figure 4b). Within the first 2 ps, the electron absorbance undergoes a blue shift, which terminates at the spectrum of solvated $e_{aq}$ observed at later times (e.g., 10 ps, Figures 2 and 5). This shift was attributed to solvation and nonadiabatic electronic relaxation of the nascent electrons.[42,43] At 10 ps, the absorbance at 660 nm is substantially larger than that observed in neat water under comparable excitation conditions, indicating that the majority of the solvated electrons is produced by photoionization of the solute.

Typical $\Delta A$ spectra at longer time delays 10, 100, and 1000 ps for $E_0 = 0.08$ and 0.31 J cm$^{-2}$ are shown in Figure 5. The most obvious change in the spectra between 10 and 1000 ps is the decay of the $e_{aq}$. As shown in Figure 6a, it exhibits a 100−200 ps component for 0.08 and 0.38 J cm$^{-2}$, respectively, while an interesting increase of the ground-state bleach also shows up (Figure 6b). This increase is larger than if it were merely caused by the decay of the overlapping absorption of solvated electrons (e.g., like in Figure 2), suggesting therefore a net decrease of the ground-state $[Ru^{II}(bpy)_3]^{2+}$ population on ∼200 ps time scale. The 510 nm absorption shoulder peak in the $\Delta A$ spectra, which was assigned to the absorption of the $[Ru^{II}(bpy)_3]^{+}$ product[44] (Figure 1b), also develops on the same time scale. The major, slower decay component of $e_{aq}$ is not fully resolved on the 1 ns time scale of this experiment. Having taken into account that the decay at 660 nm (due to the solvated electron) has an offset due to the $^3$MLCT absorption, we extract a time constant $\tau \approx 1$ ns for this slow component, which is roughly independent of excitation energy. The decrease of both ground state bleach $[Ru^{II}(bpy)_3]^{2+}$ and $e_{aq}$ population together with the buildup of the pronounced 510 nm band (thus due to the reduced species $[Ru^{II}(bpy)_3]^{+}$) is also clearly observed for the concentrated 20 mM solution. In fact, the amplitude increase of the reduced ground state from 50 ps to 1 ns could be ca. 1.5 times larger in the 20 mM solution than in the 10 mM solution at comparable initial $e_{aq}$ concentrations (thus after ca. 50 ps). However, there is less probe transmission through the concentrated (20 mM) sample yielding less accurate spectra and consequently poorer fits of the $\Delta A$ spectra to eq 3. Therefore, the yields of the product species were not systematically determined for such large solute concentrations.

**Anisotropy Measurements.** Rotational diffusion of metal-centered complexes similar to the ones considered in this work

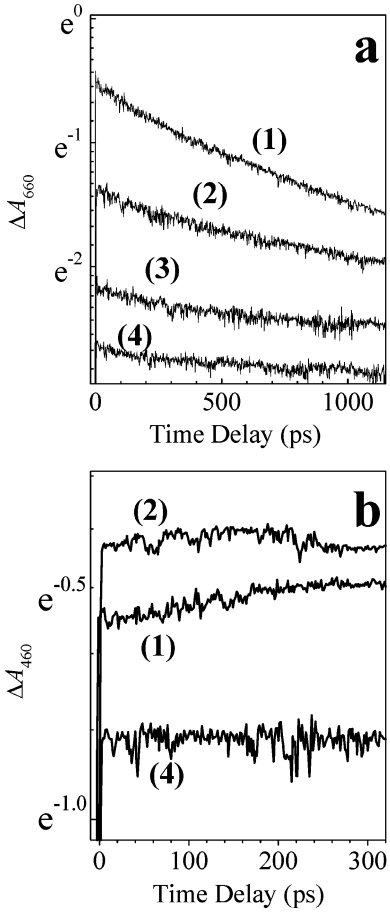


**Figure 6.** Temporal evolution of photoproducts following excitation of aqueous $[Ru^{II}(bpy)_3]^{2+}$ (10 mM) with 400 nm femtosecond laser pulses. The used excitation energies are (in J cm$^{-2}$): 0.15 (1), 0.055 (2), 0.028 (3), and 0.012 (4). (a) Probing predominantly the solvated electron ($\lambda = 660$ nm). (b) Probing predominantly the ground-state depletion ($\lambda = 460$ nm).

has often been studied in polar solvents other than water.[7,45−47] When rescaling the measured rotational periods according to the different viscosities of the used solvents with respect to that of water, we expect rotational diffusion times on a 100−150 ps time scale. The rotational diffusion time of $[Ru^{II}(bpy)_3]^{2+}$ (in $D_2O$ at 33 °C) has been measured to be 100 ps.[48] In addition, the localized electron in the $^3$MLCT state can inherently hop from one ligand to another in a process called interligand electron transfer (ILET). An early estimate by Cooley et al.[45] indicates a 15 ps time constant for ILET in aqueous $[Ru^{II}(bpy)_3]^{2+}$, but more recent direct ultrafast studies of this and similar molecules suggest that it may be much faster.[7,10,11] Both rotational diffusion and ILET change the orientation of the molecular transition dipole moment, which is probed in these experiments, and may thus affect the population dynamics on the 10−100 ps time scale investigated in this work. Therefore, special care was taken such that neither rotational diffusion nor ILET be of any importance under our conditions. We find that neither the kinetic behavior nor the quantitative appearance of the products are noticeably affected by the relative polarization of the excitation and probe electric field vectors. Two relative orientations between the excitation and probe electric field vectors were compared: perpendicular and magic angle (54.7°). We also measured the transient absorption spectra with the parallel ($\Delta A^{\parallel}$) and perpendicular ($\Delta A^{\perp}$) relative polarizations at different excitation levels, from which we constructed the anisotropy ($r$) spectra using the usual expression: $r = (\Delta A^{\parallel} - \Delta A^{\perp})/(\Delta A^{\parallel} + 2\Delta A^{\perp})$. The $r$ spectra obtained at $E_0 = 0.12$ J cm$^{-2}$ reveal very small $r$ values ($r < 0.05$) within the absorption of $^3$MLCT and ground-state complexes (Figure 2b). Much smaller values ($r \approx 0$) are obtained at larger $E_0$. The power dependence of $r$ suggests that the anisotropy values are reduced by saturation effects,[49] where the intense pump pulse excites a nearly isotropic distribution of $^3$MLCT orientations (and of the depleted ground-state concentration discussed below).

**TABLE 1: The Product Species and Their Best-fit Concentrations (Depleted Concentrations for Ground-State Molecules) at 10 ps and 1 ns Delays after Photolysis of $[Ru^{II}(bpy)_3]^{+}$ (10 mM) in Aqueous Solutions with 135 fs Laser Pulses of Various Fluence ($E_0$) Centered at 400 nm**

| | $\Delta c$ ($10^{-3}$, M) | | |
|---|---|---|---|
| | time delays (ps) | | |
| $E_0$ (J cm$^{-2}$) | 10 | 1000 | involved species[a] |
| 0.04 | 0.23 | 0.066 | $e_{aq}$ |
| | −3.02 | −3.24 | $[Ru^{II}(bpy)_3]^{2+}$ |
| | 2.98 ± 0.32 | | $[Ru^{III}(bpy^{\cdot-})(bpy)_2]^{2+}$ |
| | 0 | ≤0.028 | $[Ru^{II}(bpy)_3]^{+}$ |
| | not detected | | $[Ru^{III}(bpy)_3]^{3+}$ |
| 0.08 | 0.53 | 0.083 | $e_{aq}$ |
| | −4.73 | −4.98 | $[Ru^{II}(bpy)_3]^{2+}$ |
| | 3.98 ± 0.32 | | $[Ru^{III}(bpy^{\cdot-})(bpy)_2]^{2+}$ |
| | 0.16 | 0.48 | $[Ru^{II}(bpy)_3]^{+}$ |
| | not detected | | $[Ru^{III}(bpy)_3]^{3+}$ |
| 0.17 | 0.95 | 0.27 | $e_{aq}$ |
| | −5.90 | −6.15 | $[Ru^{II}(bpy)_3]^{2+}$ |
| | 4.32 ± 0.32 | | $[Ru^{III}(bpy^{\cdot-})(bpy)_2]^{2+}$ |
| | 0.33 | 0.58 | $[Ru^{II}(bpy)_3]^{+}$ |
| | not detected | | $[Ru^{III}(bpy)_3]^{3+}$ |
| 0.31 | 2.13 | 0.58 | $e_{aq}$ |
| | −6.60 | −6.71 | $[Ru^{II}(bpy)_3]^{2+}$ |
| | 3.98 ± 0.16 | | $[Ru^{III}(bpy^{\cdot-})(bpy)_2]^{2+}$ |
| | 0.61 | 1.05 | $[Ru^{II}(bpy)_3]^{+}$ |
| | 1.80 | 0.48 | $[Ru^{III}(bpy)_3]^{3+}$ |

[a] See Figures 7 and 8 for the temporal behavior of the species concentration.

**Analysis of Transient Absorption Spectra for $t \geq 10$ ps.** With the absolute $\sigma$ curves over the entire spectral range presented in Section II, we use eq 3 to fit the $\Delta A$ spectra of $[Ru^{II}(bpy)_3]^{2+}$ (10 mM) measured between 10 ps and 1 ns. The use of three fit parameters, the concentration changes of ground-state $[Ru^{II}(bpy)_3]^{2+}$, $^3$MLCT, and $e_{aq}$, yields fits of poor quality, which deviate significantly from the measured $\Delta A$ spectra around 380 and around 510 nm, especially at longer time delays and for larger excitation fluences. This suggests the presence of a new product species, $[Ru^{II}(bpy)_3]^{+}$, which absorbs both around 380 and 510 nm[44] (Figure 1b). The inclusion of $[Ru^{II}(bpy)_3]^{+}$ in the fitting routine (i.e., four fit parameters) greatly improves the fits, allowing us to adequately reproduce the entire $\Delta A$ curve (Figure 5). The addition of weakly absorbing $[Ru^{III}(bpy)_3]^{3+}$ to the fit improves the $\chi^2$ values to a noticeable degree, but only for the $\Delta A$ spectra measured at 0.31 J cm$^{-2}$. The best-fit concentrations of $[Ru^{III}(bpy)_3]^{3+}$ are found to be at most 15%, on average, lower than the best-fit concentrations of $e_{aq}$ at each time delay. The fact that both concentrations are correlated, even when not constrained by any specific relationship in the fit function, suggests that these two species are linked through a subsequent mechanism. A further increase in the number of product species is beyond the accuracy of our data and not necessary (see below). The species involved and their best-fit concentrations as a function of time are summarized in Table 1 and in Figures 7 and 8.

**Product Concentrations on a 10 ps Time Scale.** Because the 10 ps $\Delta A$ spectra are characteristic of the fully thermalized

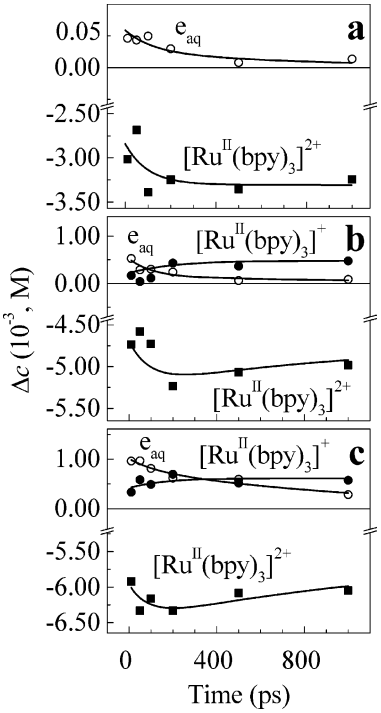


**Figure 7.** Concentrations of the depleted ground-state $[Ru^{II}(bpy)_3]^{2+}$, and of the formed products $[Ru^{II}(bpy)_3]^{+}$ and $e_{aq}$ (symbols) determined by spectral deconvolution of the transient absorption spectra of aqueous $[Ru^{II}(bpy)_3]^{2+}$ (10 mM) using eq 3. The spectra were measured at the following excitation fluence $E_0$ (in J cm$^{-2}$): 0.04 (a), 0.08 (b), and 0.17 (c). The double exponential fit curves (lines) to concentrations of the indicated species are given as a guide to the eye.

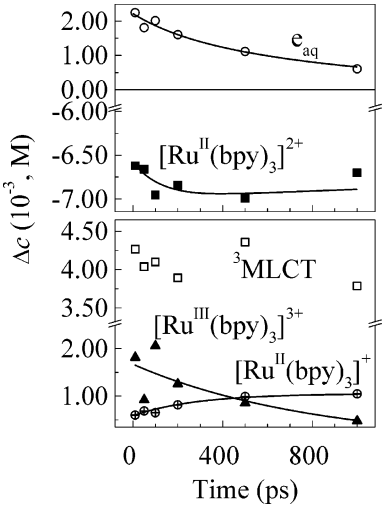


**Figure 8.** Concentrations of the depleted ground state $[Ru^{II}(bpy)_3]^{2+}$, and of the formed products $[Ru^{II}(bpy)_3]^{+}$, $[Ru^{III}(bpy)_3]^{3+}$, and $e_{aq}$ (symbols) determined from the transient absorption spectra of aqueous $[Ru^{II}(bpy)_3]^{2+}$ (10 mM) using spectral deconvolution with eq 3. The spectra were measured at $E_0 = 0.31$ J cm$^{-2}$. The double exponential fit curves (lines) to concentrations of the indicated species are given as a guide to the eye.

$^3$MLCT absorption,[37] and the energetic relaxation of nascent electrons followed by their solvation is complete on a similar time scale,[42,43] equilibrated $\sigma$ values are used to obtain the product concentrations from the $\Delta A$ spectra for $t \geq 10$ ps. We find that with increasing fluence $E_0$, the degree of depletion of both $[Ru^{II}(bpy)_3]^{2+}$and $\Delta c(^3\text{MLCT})$ tends to level off (Figure 9a). The produced amount of $e_{aq}$ follows a quasi-linear $E_0$ dependence, $\Delta c(e_{aq}) = \text{const} \cdot E_0^{1.17}$ (Figure 9b). At the highest fluence ($E_0 = 0.31$ J cm$^{-2}$), ca. 2 mM are produced in the 10 mM sample, which is 1.5 times larger than in neat water. However, the concentration of electrons produced by photoionization of water in 10 mM $[Ru^{II}(bpy)_3]^{2+}$ has to be much smaller because of the strong linear solute absorption, because its fluence corresponds to an intensity of 15 photons per MLCT cross-section on the sample surface. Further evidence that the $[Ru^{II}(bpy)_3]^{2+}$ complex is the main source of solvated electrons comes from the nearly linear dependence of the $e_{aq}$ concentration on $E_0$ for the 10 mM solution (while it is nearly cubic in neat water). Because of this linear dependence, the relative fraction of $e_{aq}$ produced by photoionization of the solvent $H_2O$ is likely to be much smaller at lower excitation fluences. The presence of an appreciable, $E_0$-dependent amount of $[Ru^{II}(bpy)_3]^{+}$ is indicated by the fits of the 10-ps $\Delta A$ spectra. At all excitation fluences ($E_0 = 0.04-0.31$ J cm$^{-2}$) and at all delay times, a roughly balanced ratio of depleted to generated populations is found, $-\Delta c([Ru^{II}(bpy)_3]^{2+})/(\Delta c(^3\text{MLCT}) + \Delta c([Ru^{II}(bpy)_3]^{+} + \Delta c([Ru^{III}(bpy)_3]^{3+}) = 1$ within ca. 10% (Table 1), indicating that these species predominantly contribute to the photochemistry 10 ps after the 400-nm excitation pulse.

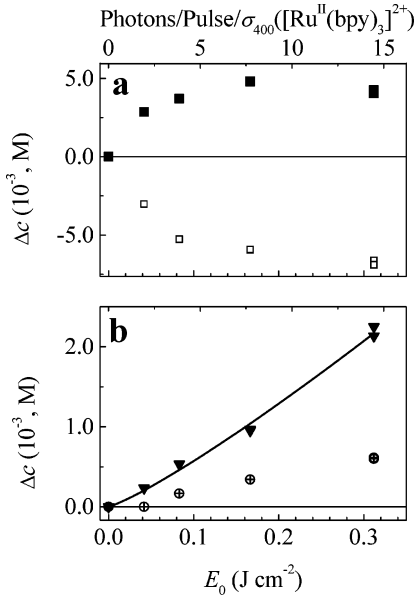


**Figure 9.** Pump fluence dependence of the photoproduct concentrations 10 ps after 400 nm photolysis of 10 mM of aqueous $[Ru^{II}(bpy)_3]^{2+}$; the top axis relates this to the number of incident photons per cross-section of the reactant at 400 nm. (a) Depleted ground-state $[Ru^{II}(bpy)_3]^{2+}$ (□) and generated $^3$MLCT (■) concentrations. (b) Produced $e_{aq}$ (▼) and $[Ru^{II}(bpy)_3]^{+}$ (⊕) concentrations. The line represents the best fit of the $e_{aq}$ concentration to the function $\alpha E_0^{\beta}$, where $\beta = 1.17$.

## IV. Discussion

In the following, we will discuss the origin of the different photoproducts that show up from the fits of our data.

**The Solvated Electron.** The emission from the initially excited $^1$MLCT state in water is found to be extremely short-lived ($\tau_{isc} = 15 \pm 10$ fs[12]) due to fast intersystem crossing to the vibrationally hot $^3$MLCT triplet manifold. Accordingly, upon intense excitation of $[Ru^{II}(bpy)_3]^{2+}$ with a 135-fs, 400-nm pulse, the initial absorption to $^1$MLCT can be subsequently followed by absorption of one (or more) 400-nm photon(s) of the same pulse from both the unrelaxed $^1$MLCT and/or $^3$MLCT states. The induced absorption at 400 nm observed on the leading edge (−50 fs) of the excitation pulse (Figure 2a) is likely due to the spectral signature of the nascent $^1$MLCT or $^3$MLCT state. Population can build up in the $^1$MLCT state at high femtosecond pulse intensities ($I_0 \approx (1-4) \times 10^{30}$ photons cm$^{-2}$ s$^{-1}$), because

the GS $\xrightarrow{400\text{nm}}$ $^1$MLCT first-order excitation rate constant ($\sigma$-$([Ru^{II}(bpy)_3]^{2+})_{400}I_0 = \sim(2.5-10) \times 10^{13}$ s$^{-1}$) is comparable to $^1$MLCT decay rate ($1/\tau_{isc} = 6.7 \times 10^{13}$ s$^{-1}$). Given the appreciable excited-state absorption at 400 nm at early times (Figure 2a), the probability to absorb a second photon at early times in a (1 + 1) resonant excitation process (via $^1$MLCT) is high at these fluences. At lower fluences, the $^1$MLCT absorption contribution becomes small and the population of the nascent $^3$MLCT state following intersystem crossing within the 135 fs pulse width becomes dominant. Because the ISC occurs at constant energy,[12] the subsequent absorption of a 400 nm photon by the $^3$MLCT state within the pump pulse will populate doubly excited, triplet ($^3[Ru^{III}(bpy)_2(bpy^{\cdot-*})]^{2+}$) state, located around 6.2 eV above the ground state. Large oscillator strengths for the triplet−triplet absorption (large excited-state absorption cross-section of the $^3$MLCT state, $\sigma_{400}(^3\text{MLCT}) = 2.4 \times 10^{-17}$ cm$^2$, Figure 1b) may offer a distinct possibility of the population buildup in the doubly excited triplet state, maybe even with some absorption probability of a third photon. Our observation of the solvated electron 2 ps after photolysis of $[Ru^{II}(bpy)_3]^{2+}$ strongly supports the hypothesis of prompt photoionization of this complex following the occurrence of high-intensity photochemical pathways. Finally, the appearance of the oxidized species $[Ru^{III}(bpy)_3]^{3+}$ at relatively early times (~10 ps) supports the original interpretation[50] that this species is a direct product of the photoionization process.

At 10 ps, the concentration of depleted $[Ru^{II}(bpy)_3]^{2+}$ species is nearly equal to the sum of concentrations of the three identified products ($^3$MLCT, $[Ru^{II}(bpy)_3]^{+}$, $[Ru^{III}(bpy)_3]^{3+}$, next to the byproduct $e_{aq}$) at all excitation energies used (Table 1). This implies that essentially all higher-lying excited states (coupled to $^{1,3}$MLCT at 400 nm) have relatively short lifetimes (≪10 ps). One (or more) of these states is the electron precursor state with a lifetime <2 ps. The solvated electron detected in previous UV photolysis experiments using micro- and nanosecond pulses[19,50−53] was ascribed to 2-photon photoionization via the $^3$MLCT intermediate, because of the fast decay rate of $^1$MLCT. Furthermore, the absorption of a second photon within the micro- and nanosecond long pulses can occur only from the relaxed $^3$MLCT state, because the vibrational energy relaxation rates (>$10^{11}$ s$^{-1}$) are much larger than the typical pump rates in these studies ($\sigma_{UV}I_0 \leq 3 \times 10^9$ s$^{-1}$). The lowest photon energy for which solvated electrons were observed in biphotonic nanosecond photolysis studies of $[Ru^{II}(bpy)_3]^{2+}$ is 3.50 eV (a 355-nm excitation wavelength).[19,51] Taking into account the ultrafast ISC and relaxation in the $^3$MLCT state, the second photon acts on the thermalized $^3$MLCT state located 2.12 eV[1] above the ground state. Thus, in total 3.50 eV + 2.12 eV = 5.62 eV represents a lower boundary for the ionization energy of $[Ru^{II}(bpy)_3]^{2+}$. Long-pulse photolysis with $\lambda \geq 400$ nm (≤3.1 eV) was found inefficient in the production of $e_{aq}$[50] (thus with 3.1 eV + 2.12 eV = 5.22 eV), and the ionization threshold lies therefore between 5.22 and 5.62 eV above the ground state. In this work, with femtosecond 400 nm pulse excitation, the (1 + 1) excitation ($E_{exc} = 6.2$ eV) through the nonthermalized $^1$MLCT and $^3$MLCT manifolds is in excess of these values and is sufficient to generate electrons from the solute. For a stepwise two-photon absorption to an electron precursor state, a nearly linear increase of the concentration of $e_{aq}$ with photolysis energy suggests saturation of one of the two involved transitions.[54] Already, the $^1$MLCT transition is saturated, so that the $e_{aq}$ may be produced by means of one-(400 nm)-photon (unsaturated) absorption from the $^1$MLCT. Eventually, for the three-photon absorption, presumably the second step from $^3$MLCT is driven into saturation relatively quickly (large $\sigma_{400}(^3\text{MLCT})$). At all (high) intensities used in this study, these two scenarios seem to be possible. In the case when the pulse duration (135 fs, fwhm) is long as compared to the $^1$MLCT lifetime ($\tau_{isc} \approx 15$ fs), the GS $\xrightarrow{400\text{nm}}$ $^1$MLCT transition is saturated by the intensity of the excitation pulse. The population of these two levels equalizes when the saturation parameter, $\sigma 400([Ru^{II}(bpy)3]^{2+})I_0\tau_{isc}$, becomes much greater than unity. For the peak irradiance $I_0$ in the range (0.56−4.35) × $10^{30}$ photons cm$^{-2}$ s$^{-1}$, and $\sigma 400([Ru^{II}(bpy)3]^{2+}) = 2.3 \times 10^{-17}$ cm$^2$, the saturation parameter accepts values from 0.2 to 1.5.

**The Reduced Species $[Ru^{II}(bpy)_3]^{+}$.** It may arise from a reduction mechanism involving a highly electronically excited $[Ru^{II}(bpy)_3]^{2+}$ acceptor and a nearby water molecule donor on a 100 fs time scale. Using the Rehm−Weller equation, the corresponding driving force is estimated to be $\Delta G^\circ \approx 7.28 - E_{0-0}$. Indeed, the involved free energy is: $\Delta G^\circ = E^0[H_2O^+/H_2O] - E^0[Ru^{II}(bpy)_3{}^{2+}/Ru^{II}(bpy)_3{}^{+}] - E_{0-0} + W_p - W_r$, where $E^0[Ru^{II}(bpy)_3{}^{2+}/Ru^{II}(bpy)_3{}^{+}]$ is the acceptor ground state reduction potential (−1.26 V in $H_2O$ versus normal hydrogen electrode, NHE),[1] $E^0[H_2O^+/H_2O]$ is the donor oxidation potential, $E_{0-0}$ is the purely electronic excitation energy of the acceptor state, and $W_p$ and $W_r$ represent the work required to bring reactants and products together (neglected in strongly polar solvents following standard practice). The $E^0[H_2O^+/H_2O]$ value is estimated using the correlation between oxidation potentials and gas-phase ionization potentials (IP) by Miller et al.,[55] $E^0$-$[A^+/A] = 0.89\text{IP} - 5.51$ (vs NHE). For $H_2O$, IP = 12.96 eV.[56] Therefore, electron transfer from water to excited $[Ru^{II}(bpy)_3]^{2+}$ is energetically feasible for excitation energies larger than 7.28 eV. This is available through three 400 nm photon absorption ($E_{exc} = 9.3$ eV), and the highly excited state(s) involved, possibly Rydberg-like charge-transfer-to-solvent excited states of large spatial extent, should be very short-lived, consistent with the ~100 fs observation time scale.

We observed further development of reduced $[Ru^{II}(bpy)_3]^{+}$ on a 100−200 ps time scale. It is very likely that, following the photoionization of $[Ru^{II}(bpy)_3]^{2+}$, the photoelectron is ejected away from the parent cation to a large distance $r_0$ with a broad distance distribution by analogy with the studies of multiphoton ionization of neat water and resonant one-photon electron detachment from mono- and polyvalent anions.[54,57,58] Photoelectrons with less than 1 eV excess kinetic energy (near-threshold photoionization) are thought to localize ca. 10−15 Å from the parent species on a subpicosecond time scale.[54,57,59] For high-energy photoionization, the electrons are promoted into the water conduction band, producing delocalized,[41] conduction band electrons that can migrate to a length of more than 35 Å from the original site.[60] Given the conduction band gap of water and energetics of a hydrated electron,[61] the ionization threshold for $[Ru^{II}(bpy)_3]^{2+}$, and the total energy in the excitation process, the two-photon photoionization of $[Ru^{II}(bpy)_3]^{2+}$ is expected to be near-threshold, whereas in the three-photon photoionization the electrons are transferred into the conduction band. The most-probable solute nearest-neighbor distance can be estimated via $r_{mp} = (2\pi\rho)^{-1/3}$, where $\rho$ is the $[Ru^{II}(bpy)_3]^{2+}$ number density in solution. At 10 and 20 mM, $r_{mp} = 30$ and 24 Å, respectively. It is reasonable to assume that some electrons are photoejected closer to adjacent $[Ru^{II}(bpy)_3]^{2+}$ cations forming solvent-separated contact pairs, and thus react via eq 7 (see below) with faster rates than observed for the bulk homogeneous diffusion kinetics. This explanation is consistent with the fact that the ~1.5 times increase of the $[Ru^{II}(bpy)_3]^{+}$ product concentration

50 ps onward is observed upon increasing the solute concentration from 10 to 20 mM. The formation of $[Ru^{II}(bpy)_3]^+$ on this time scale is not observed in the excited, dilute samples (0.4 mM), as expected. Therefore, the reduction observed from ten picoseconds to a few hundred picoseconds can be rationalized via the combination of the ejected electron with nearby-lying ground state molecules.

**Long-Lived Photoproduct Species.** With respect to the observed concentration changes on the 1 ns time scale, we discuss the following scenarios: next to eqs 1 and 2 describing the photoexcitation process and ignoring the $e_{aq}$ photogeneration details, we have to consider the reactions:

$$^{1,3}\mathrm{MLCT} \xrightarrow{h\nu} [Ru^{III}(bpy)_3]^{3+} + e_{aq} \quad (6)$$

$$[Ru^{II}(bpy)_3]^{2+} + e_{aq} \xrightarrow{(5.2 \div 8.2) \times 10^{10}\ M^{-1}\ s^{-1}} [Ru^{II}(bpy)_3]^{+}\ ^{50,62} \quad (7)$$

$$^{3}\mathrm{MLCT} + [Ru^{II}(bpy)_3]^{2+} \xrightarrow{(5.1 \pm 0.4) \times 10^{7}\ M^{-1}\ s^{-1}} 2[Ru^{II}(bpy)_3]^{2+}\ ^{5} \quad (8)$$

$$^{3}\mathrm{MLCT} + {}^{3}\mathrm{MLCT} \xrightarrow{(1.1 \pm 0.3) \times 10^{8}\ M^{-1}\ s^{-1}} [Ru^{II}(bpy)_3]^{+} + [Ru^{III}(bpy)_3]^{3+}\ ^{5} \quad (9)$$

$$e_{aq} + e_{aq} + 2H_2O \xrightarrow{5.5 \times 10^{9}\ M^{-1}\ s^{-1}} H_2 + 2OH^-\ ^{63} \quad (10)$$

$$[Ru^{III}(bpy)_3]^{3+} + [Ru^{II}(bpy)_3]^{+} \xrightarrow{(3.4 \pm 0.3) \times 10^{9}\ M^{-1}\ s^{-1}} 2[Ru^{II}(bpy)_3]^{2+}\ ^{22} \quad (11)$$

$$[Ru^{III}(bpy)_3]^{3+} + e_{aq} \xrightarrow{(5.2 \pm 0.4) \times 10^{10}\ M^{-1}\ s^{-1}} [Ru^{II}(bpy)_3]^{2+}, {}^{3}\mathrm{MLCT}, \text{“isolated state”}\ ^{22} \quad (12)$$

Reactions 8−11, with second-order rate constants in the range $(0.05-3.4) \times 10^9\ M^{-1}\ s^{-1}$ at room temperature,[5,22,63] should occur on a submicrosecond to microsecond time scale (at the millimolar concentrations of the involved species), and are thus disregarded on the 1-ns time scale studied here. Reactions 7 and 12 are comparatively fast. Second-order rate constants of $8.2 \times 10^{10}\ M^{-1}\ s^{-1}$ [62] and $5.6 \times 10^{10}\ M^{-1}\ s^{-1}$ [50] have been reported for the reduction of ground-state $[Ru^{II}(bpy)_3]^{2+}$ by $e_{aq}$ (eq 7). Assuming an average ejection distance of the solvated electron around 25 Å (see above), these rates correspond to a reduction time around 200 ps, as observed in this experiment. We also observe that the fast decay of $e_{aq}$ on a ∼200 ps time scale is concurrent with the buildup of reduced $[Ru^{II}(bpy)_3]^+$ and with the loss of ground-state $[Ru^{II}(bpy)_3]^{2+}$, indicating the presence of reaction 7. Combining the published rate constant with the extended electron ejection distance, we find a nice agreement with the observed formation rate of around 200 ps. Note that the diffusion-controlled reaction 7 depends on temperature, but even assuming that 100% of the absorbed energy is released as heat, the maximum average temperature jump in the photolyzed volume at our highest $E_0$ (0.31 J cm$^{-2}$) can be estimated to be ∼10 K; this heat release is roughly 1/15 of that required to explain the observed kinetic behavior.

Another key observation is that the slow decay of $e_{aq}$ is concomitant with the decay of $[Ru^{III}(bpy)_3]^{3+}$ ($\tau \approx 800$ ps), which may be assigned to recombination (back electron transfer). We observe no evidence for a fast ($2\ \mathrm{ps} < t < 200\ \mathrm{ps}$) recombination. This is probably because some photoelectrons are distributed farther away from the parent cation and because, as the electron carries away the energy in excess of the ionization threshold (∼5.62 eV), the larger radius geminate pairs are produced at larger excess excitation energies. The ions thermalize quickly after excitation (within a few picoseconds in polar solvents[64,65]); therefore, the outcome of the recombination of $[Ru^{III}(bpy)_3]^{3+}$ and $e_{aq}$ could be expected to be the same as for their diffusion encounter (eq 12). This encounter leads to ground-state $[Ru^{II}(bpy)_3]^{2+}$, $^3$MLCT, and another, longer lived dark state that does not convert to $^3$MLCT with the corresponding yields 7%, 38%, and 55%, respectively.[23] Let us translate these yields into the product concentrations. For example, for $E_0 = 0.31$ J cm$^{-2}$, the concentration of $e_{aq}$ and $[Ru^{III}(bpy)_3]^{3+}$ that recombine is ∼1.6 mM. The “isolated” dark state would be produced in the concentration of ∼0.88 mM for a 55% yield, which approximately corresponds to the observed shortage on the product side (∼1.25 mM) in the concentration balance at 1 ns. Finally, we note that the fast decay component of $\Delta c(e_{aq})$ becomes relatively less pronounced with increased $E_0$, suggesting that the recombination (eq 12) becomes dominant over the reduction (eq 7). This may be attributed to the increase of the absolute number of recombination partners, and the decrease of the relative importance of eq 7 with the majority of $[Ru^{II}(bpy)_3]^{2+}$ being in the product states.

One of the aims of this study was a better characterization of the behavior of aqueous $[Ru^{II}(bpy)_3]^{2+}$ under high-intensity femtosecond laser pulses at 400 nm in time-resolved X-ray absorption spectroscopy (XAS) experiments carried out with 70 ps X-ray pulses.[66−68] From the present optical studies, we find that the concentration balance between the depleted ground state $[Ru^{II}(bpy)_3]^{2+}$ species, and only three product species formed 10 ps after the 400 nm excitation pulse, is maintained to within 10%, even at the very high power density of 2.15 TW cm$^{-2}$ (which is similar to the one used in the time-resolved XAS study[68]). In addition, the $^3$MLCT state remains the dominant photoproduct (to >66%), thus supporting the analysis of the transient XAS data presented in ref 68.

## V. Conclusions

We have performed a transient absorption study on the photochemistry of aqueous $[Ru^{II}(bpy)_3]^{2+}$ under a high-intensity femtosecond laser excitation. The photolysis of $[Ru^{II}(bpy)_3]^{2+}$ (10 and 20 mM) with 400 nm, 135 fs pulses of varying power density (up to 2.15 TW cm$^{-2}$) leads to the following photoproducts: the complex in the $^3$MLCT triplet excited state ($[Ru^{III}(bpy)_2(bpy^{\cdot-})]^{2+}$), the oxidized form $[Ru^{III}(bpy)_3]^{3+}$, the reduced species $[Ru^{II}(bpy)_3]^+$, and the solvated electrons $e_{aq}$. The precursor excited states for the nascent electrons are accessed by stepwise multiphoton processes via the nonthermalized $^1$MLCT and $^3$MLCT states. The thermalized solvated electron, $e_{aq}$, is observed 2 ps after photoexcitation, in agreement with similar photoionization studies in aqueous solutions. The fast formation of $[Ru^{III}(bpy)_3]^{3+}$, a byproduct of photoionization, is confirmed by spectral deconvolution of the 10 ps transient absorption spectra, which rules out its formation via bimolecular reactions of the photoproducts. The same spectral analysis enables the observation of a noticeable amount of the $[Ru^{II}(bpy)_3]^+$ product. The analysis of the transient absorption spectra also shows (i) the decay of $e_{aq}$, the loss of ground state $[Ru^{II}(bpy)_3]^{2+}$, and the build-up of $[Ru^{II}(bpy)_3]^+$ all occur on the ∼200 ps time scale, and (ii) a slower decay component of $e_{aq}$ and $[Ru^{III}(bpy)_3]^{3+}$ with a ∼1 ns time constant due to recombination with each other. We propose that, following photoionization of $[Ru^{II}(bpy)_3]^{2+}$, geminate pairs with a broad

distribution of radii are produced due to significant excess energies available in the multiphoton excitation processes. Some of the nascent photoelectrons form solvent-separated contact pairs with the adjacent ground-state $[Ru^{II}(bpy)_3]^{2+}$ neighbors, giving rise to $[Ru^{II}(bpy)_3]^{+}$ on the 100−200 ps time scale. Thus, the $[Ru^{II}(bpy)_3]^{+}$ product is formed via two different mechanisms on two different time scales. While the $^3$MLCT is the major product and $[Ru^{II}(bpy)_3]^{+}$ is the substantial product out to the largest delay times explored in this experiment (1 ns), $e_{aq}$ and $[Ru^{III}(bpy)_3]^{3+}$ are substantial products around 10 ps after photolysis but become peripheral products at 1 ns.

**Acknowledgment.** We thank Dr. M. Kaiser for his help with the data format conversion program. This work was funded by the Swiss National Science Foundation via contracts 620-066145 and 20-6791202. We acknowledge the Integrative Initiative of Infrastructure project LASERLAB-EUROPE, contract RII3-CT-2003-506350, that enables us to access the ultrafast laser facilities of the Department of Chemical Physics (Lund University, Sweden), where some of the reported experiments were performed.

## References and Notes

(1) Juris, A.; Balzani, V.; Barigelletti, F.; Campagna, S.; Belser, P.; Vonzelewsky, A. *Coord. Chem. Rev.* **1988**, *84*, 85.
(2) Vlcek, A. *Coord. Chem. Rev.* **2000**, *200*, 933.
(3) Kalyanasundaram, K. *Coord. Chem. Rev.* **1982**, *46*, 159.
(4) Creutz, C.; Chou, M.; Netzel, T. L.; Okumura, M.; Sutin, N. *J. Am. Chem. Soc.* **1980**, *102*, 1309.
(5) Milosavljevic, B. H.; Thomas, J. K. *J. Phys. Chem.* **1983**, *87*, 616.
(6) Damrauer, N. H.; Cerullo, G.; Yeh, A.; Boussie, T. R.; Shank, C. V.; McCusker, J. K. *Science* **1997**, *275*, 54.
(7) Shaw, G. B.; Brown, C. L.; Papanikolas, J. M. *J. Phys. Chem. A* **2002**, *106*, 1483.
(8) Shaw, G. B.; Papanikolas, J. M. *J. Phys. Chem. B* **2002**, *106*, 6156.
(9) Bhasikuttan, A. C.; Suzuki, M.; Nakashima, S.; Okada, T. *J. Am. Chem. Soc.* **2002**, *124*, 8398.
(10) Wallin, S.; Davidsson, J.; Modin, J.; Hammarstrom, L. *J. Phys. Chem. A* **2005**, *109*, 4697.
(11) Wallin, S.; Davidsson, J.; Modin, J.; Hammarstrom, L. *J. Phys. Chem. A* **2005**, *109*, 9378.
(12) Cannizzo, A.; van Mourik, F.; Gawelda, W.; Zgrablic, G.; Bressler, C.; Chergui, M. *Angew. Chem., Int. Ed.* **2006**, *45*, 3174.
(13) Demas, J. N.; Crosby, G. A. *J. Am. Chem. Soc.* **1971**, *93*, 2841.
(14) Vanhouten, J.; Watts, R. J. *J. Am. Chem. Soc.* **1975**, *97*, 3843.
(15) Tsushima, M.; Ikeda, N.; Nozaki, K.; Ohno, T. *J. Phys. Chem. A* **2000**, *104*, 5176.
(16) Ikeda, N.; Yoshimura, A.; Tsushima, M.; Ohno, T. *J. Phys. Chem. A* **2000**, *104*, 6158.
(17) Ferraudi, G.; Arguello, G. A. *Inorg. Chim. Acta* **1988**, *144*, 53.
(18) Thompson, D. W.; Wishart, J. F.; Brunschwig, B. S.; Sutin, N. *J. Phys. Chem. A* **2001**, *105*, 8117.
(19) Goez, M.; Schiewek, M.; Musa, M. H. O. *Angew. Chem., Int. Ed.* **2002**, *41*, 1535.
(20) Goez, M.; von Ramin-Marro, D.; Musa, M. H. O.; Schiewek, M. *J. Phys. Chem. A* **2004**, *108*, 1090.
(21) Yeh, A. T.; Shank, C. V.; McCusker, J. K. *Science* **2000**, *289*, 935.
(22) Jonah, C. D.; Matheson, M. S.; Meisel, D. *J. Am. Chem. Soc.* **1978**, *100*, 1449.
(23) Balzani, V.; Juris, A.; Venturi, M.; Campagna, S.; Serroni, S. *Chem. Rev.* **1996**, *96*, 759.
(24) Murov, S. L.; Hug, G. L.; Carmichael, I. *Handbook of Photochemistry*, 2nd ed.; M. Dekker: New York, 1993.
(25) Rasmusson, M.; Tarnovsky, A. N.; Akesson, E.; Sundstrom, V. *Chem. Phys. Lett.* **2001**, *335*, 201.
(26) Kovalenko, S. A.; Dobryakov, A. L.; Ruthmann, J.; Ernsting, N. P. *Phys. Rev. A* **1999**, *59*, 2369.
(27) Kovalenko, S. A.; Ernsting, N. P.; Ruthmann, J. *Chem. Phys. Lett.* **1996**, *258*, 445.
(28) Pommeret, S.; Gobert, F.; Mostafavi, A.; Lampre, I.; Mialocq, J. C. *J. Phys. Chem. A* **2001**, *105*, 11400.
(29) Bonneau, R.; Carmichael, I.; Hug, G. L. *Pure Appl. Chem.* **1991**, *63*, 290.
(30) Bensasson, R.; Salet, C.; Balzani, V. *J. Am. Chem. Soc.* **1976**, *98*, 3722.
(31) Kalyanasundaram, K.; Neumannspallart, M. *Chem. Phys. Lett.* **1982**, *88*, 7.
(32) Miedlar, K.; Das, P. K. *J. Am. Chem. Soc.* **1982**, *104*, 7462.
(33) Ohno, T.; Yoshimura, A.; Mataga, N. *J. Phys. Chem.* **1990**, *94*, 4871.
(34) Braterman, P. S.; Harriman, A.; Heath, G. A.; Yellowlees, L. J. *J. Chem. Soc., Dalton Trans.* **1983**, 1801.
(35) Rougee, M.; Ebbesen, T.; Ghetti, F.; Bensasson, R. V. *J. Phys. Chem.* **1982**, *86*, 4404.
(36) Hauser, A.; Krausz, E. *Chem. Phys. Lett.* **1987**, *138*, 355.
(37) Lachish, U.; Infelta, P. P.; Gratzel, M. *Chem. Phys. Lett.* **1979**, *62*, 317.
(38) Yoshimura, A.; Hoffman, M. Z.; Sun, H. *J. Photochem. Photobiol., A* **1993**, *70*, 29.
(39) Ohno, T.; Yoshimura, A.; Prasad, D. R.; Hoffman, M. Z. *J. Phys. Chem.* **1991**, *95*, 4723.
(40) Mcgowen, J. L.; Ajo, H. M.; Zhang, J. Z.; Schwartz, B. J. *Chem. Phys. Lett.* **1994**, *231*, 504.
(41) Crowell, R. A.; Lian, R.; Shkrob, I. A.; Qian, J.; Oulianov, D. A.; Pommeret, S. *J. Phys. Chem. A* **2004**, *108*, 9105.
(42) Yokoyama, K.; Silva, C.; Son, D. H.; Walhout, P. K.; Barbara, P. F. *J. Phys. Chem. A* **1998**, *102*, 6957.
(43) Assel, M.; Laenen, R.; Laubereau, A. *J. Chem. Phys.* **1999**, *111*, 6869.
(44) Mulazzani, Q. G.; Emmi, S.; Fuochi, P. G.; Hoffman, M. Z.; Venturi, M. *J. Am. Chem. Soc.* **1978**, *100*, 981.
(45) Cooley, L. F.; Bergquist, P.; Kelley, D. F. *J. Am. Chem. Soc.* **1990**, *112*, 2612.
(46) Henseler, A.; Vauthey, E. *Chem. Phys. Lett.* **1994**, *228*, 66.
(47) Cushing, J. P.; Butoi, C.; Kelley, D. F. *J. Phys. Chem. A* **1997**, *101*, 7222.
(48) Masuda, Y.; Yamatera, H. *J. Phys. Chem.* **1984**, *88*, 3425.
(49) Albrecht, A. C. *J. Mol. Spectrosc.* **1961**, *6*, 84.
(50) Meisel, D.; Matheson, M. S.; Mulac, W. A.; Rabani, J. *J. Phys. Chem.* **1977**, *81*, 1449.
(51) Atherton, S. J. *J. Phys. Chem.* **1984**, *88*, 2840.
(52) Naik, D. B.; Schnabel, W. *Chem. Phys. Lett.* **1994**, *228*, 616.
(53) Naik, D. B.; Schnabel, W. *Chem. Phys. Lett.* **1999**, *315*, 416.
(54) Kloepfer, J. A.; Vilchiz, V. H.; Lenchenkov, V. A.; Germaine, A. C.; Bradforth, S. E. *J. Chem. Phys.* **2000**, *113*, 6288.
(55) Miller, L. L.; Mayeda, E. A.; Nordblom, G. D. *J. Org. Chem.* **1972**, *37*, 916.
(56) *CRC Handbook of Chemistry and Physics*, 80th ed.; Lide, D., Ed.; CRC Press: Boca Raton, FL, 1999.
(57) Vilchiz, V. H.; Kloepfer, J. A.; Germaine, A. C.; Lenchenkov, V. A.; Bradforth, S. E. *J. Phys. Chem. A* **2001**, *105*, 1711.
(58) Kambhampati, P.; Son, D. H.; Kee, T. W.; Barbara, P. F. *J. Phys. Chem. A* **2002**, *106*, 2374.
(59) Kloepfer, J. A.; Vilchiz, V. H.; Lenchenkov, V. A.; Bradforth, S. E. *Liq. Dyn.* **2002**, *820*, 108.
(60) Son, D. H.; Kambhampati, P.; Kee, T. W.; Barbara, P. F. *Chem. Phys. Lett.* **2001**, *342*, 571.
(61) Coe, J. V.; Earhart, A. D.; Cohen, M. H.; Hoffman, G. J.; Sarkas, H. W.; Bowen, K. H. *J. Chem. Phys.* **1997**, *107*, 6023.
(62) Baxendal, Jh.; Fiti, M. *J. Chem. Soc., Dalton Trans.* **1972**, 1995.
(63) Buxton, G. V.; Greenstock, C. L.; Helman, W. P.; Ross, A. B. *J. Phys. Chem. Ref. Data* **1988**, *17*, 513.
(64) Whitnell, R. M.; Wilson, K. R.; Hynes, J. T. *J. Phys. Chem.* **1990**, *94*, 8625.
(65) Whitnell, R. M.; Wilson, K. R.; Hynes, J. T. *J. Chem. Phys.* **1992**, *96*, 5354.
(66) Saes, M.; Gawelda, W.; Kaiser, M.; Tarnovsky, A.; Bressler, Ch.; Chergui, M.; Johnson, S. L.; Grolimund, D.; Abela, R. *Synchrotron Radiation News* **2003**, *16*, 12.
(67) Saes, M.; Bressler, C.; Abela, R.; Grolimund, D.; Johnson, S. L.; Heimann, P. A.; Chergui, M. *Phys. Rev. Lett.* **2003**, 90.
(68) Gawelda, W.; Johnson, M.; de Groot, F. M. F.; Abela, R.; Bressler, C.; Chergui, M. *J. Am. Chem. Soc.* **2006**, *128*, 5001.